Int. J. Electrochem. Sci., 16 **(2021)** Article ID: 210947, doi: 10.20964/2021.08.31

International Journal of
ELECTROCHEMICAL
SCIENCE
www.electrochemsci.org

Effect of Oxygen Differential Aeration on Iron Corrosion Mechanism

Yingwei Liu[*], *Xinghao Li*

College of Materials Science and Chemical Engineering, Harbin Engineering University, Harbin, PR China, 150001
[*]E-mail: lywbanner@163.com

Received: 2 April 2021 / *Accepted:* 27 May 2021 / *Published:* 10 August 2021

It is very challenging to study differential concentration corrosion (DCC) mechanism through an experimental method because of the constrained space and geometric complexity in a Z-shaped pipe. Therefore, in this study, numerical modelling was applied to investigate DCC in a Z-shaped pipe. The oxygen concentration distribution in the ionic conductive layer near the pipe wall is firstly calculated. Then, based on the ionic conductive layer, the natural corrosion potential and current density of the surface unit are calculated according to the oxygen concentration. Finally, according to Kirchhoff's Second Law, the discrete equations of the corrosion potential of the ionic conductive layer are derived. The solution of these equations are the corrosion potential of the unit after polarization and the corrosion current density distribution on the pipe surface. Calculated results show that in the elbow region of a Z-shaped pipe, without considering DCC in the calculation, the calculated natural corrosion potential and current density in the condition of high oxygen concentration become high, and vice versa. But, if DCC is considered, the anodic polarization occurs at the location with low natural corrosion potential, increasing the corrosion rate; the cathodic polarization occurs at the location with high natural corrosion potential, reducing the corrosion current. The polarization greatly changes the distribution of the corrosion current so that the corrosion potential tends to homogenize. This study helps clarify the corrosion mechanism of elbow in a Z-shaped pipe and explain the reason for an early damage of the extrados of pipe elbow rather than intrados region.

Keywords: Corrosion; Differential concentration corrosion; Polarization; Z-shaped pipe; Finite element method.

1. INTRODUCTION

Differential concentration corrosion (DCC) is an important corrosion mechanism. This kind of corrosion only occurs when the oxygen differential concentration in the solution reaches a certain level. The laboratory-scale study on DCC is difficultly conducted. Currently, hanging film in laboratory

conditions is the only method to determine different oxygen concentrations for DCC study, which cannot fully reflect engineering practical conditions [1-5]. Using a pipe as an example, due to complicated internal fluid flow in the pipe, particularly drastic flow changes at pipe tees and bends, an uneven distribution of oxygen concentration can easily occur to cause a concentration corrosion. If oxygen concentration distribution is ignored in the study, the corrosion cannot be properly evaluated. Based on an analysis of over 2,000 pipeline components of Taiwan's PWR nuclear power plant, it is found that ~70% of the pipelines were firstly damaged or severely thinned at the extrados of pipe elbow [6], which obviously contradicts the traditional FAC theory. According to the traditional FAC theory [7-11], the fluid velocity near the intrados of pipe elbow is faster, causing a thinner boundary layer and a greater shear force on the wall. This flow behavior helps accelerating oxygen transport [12] and tends to cause faster electrochemical reactions. In this regard, the intrados of pipe elbow should be firstly destroyed. This abnormal phenomenon can be well explained through DCC mechanism.

Because a Z-shaped pipe is commonly used for fluid transport and DCC easily occurs at the elbow region of pipe.So, on the basis of reference[13], although that research is only on straight pipe, a DCC model about Z-shaped pipe was puts forward to clarify the mechanism.In the following sections, this process will be elaborated step by step.

2. DIFFERENTIAL CONCENTRATION CORROSION MECHANISM

According to the characteristics of fluid flow in a pipe, the flow field can be divided into two regions: the turbulent zone P at the center of the pipe and the boundary layer Q,with thickness δ (Refer to Table 2 for specific data),near the pipe wall surface as shown in Figure 1.The boundary layer can further be divided into viscous sublayer, buffer layer and logarithmic law layer. Due to the adhesion of the wall surface, the fluid flow in the viscous sublayer is laminar with a thickness of δ_B (as shown in Figure 2). Only in viscous sublayer, the following eletrochemical reactions between sublayer and the pipe wall can occur:

$$Fe \rightarrow 2Fe^{2+}+4e \quad (1)$$

$$O_2+2H_2O+4e \rightarrow 4OH^{-1} \quad (2)$$

The equilibrium potential, exchange current density and Tafel slope of reaction (1) and (2) are $E_{e,a}$、$I_{0,a}$、β_a and $E_{e,c}$、$I_{0,c}$、β_c and are listed in Table1.For the cathodic equilibrium reaction (2), the equilibrium potential and exchange current density are based on the standard oxygen concentration of $c_{O_2,0}$ listed in Table 3. If the oxygen concentration deviates from the standard value,the equilibrium potential and exchange current density should be defined by formulas(3) and(4)[14].

$$E_{e,c}^1 = E_{e,c} + \frac{RT}{nF}\ln(\frac{c_{o_{2,1}}}{c_{o_2,0}}) \quad (3)$$

$$I_{0,c}^1 = I_{0,c}(\frac{c_{o_{2,1}}}{c_{o_2,0}}) \quad (4)$$

Where $c_{O_2,1}$ is the actual oxygen concentration in liquid.

In fact ,the reactions (1) and (2) are coupled, leading to a mixed potential E_{corr} and current I_{corr}

[15]:

$$E_{corr} = \frac{1}{\beta_a + \beta_c}[(\beta_a E_{e,c} + \beta_c E_{e,a}) - \beta_a \beta_c \ln(\frac{I_{0,a}}{I^1_{0,c}})] \quad (5)$$

$$I_{corr} = I_{0,a}^{\frac{\beta_a}{\beta_a+\beta_c}} I^1_{0,c}{}^{\frac{\beta_c}{\beta_a+\beta_c}} \exp(\frac{E_{e,c} - E_{e,a}}{\beta_a + \beta_c}) \quad (6)$$

I_{corr} is the corrosion current somewhere on the wall.

Table 1. Electrochemical parameters

Parameter	Iron	Oxgyen
Equilibrium potential (V)	-0.648	0.456
Tafel slope (V/m)	0.04	0.105
Exchange current degree (A/m^2)	2.7×10^{-7}	4×10^{-9}
Conductivity(S)	4.863	

Table 2. Geometric parameters of Z-shaped pipe and sublayer thickness

L, m	R, m	r, m	δ, m
1.0	0.15	0.05	1.1×10^{-4}

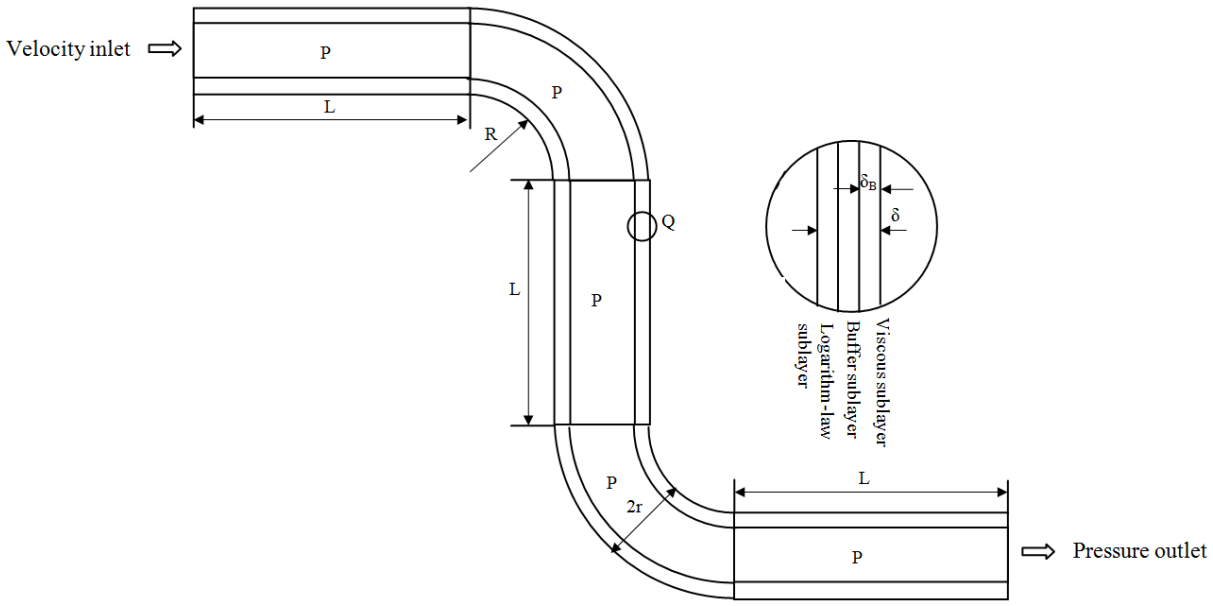

Figure 1. Schematic of Z-shaped pipe geometry and boundary conditions

The oxygen concentration at different positions in the viscous sublayer is different. Therefore, the viscous sublayer is artificially divided into many small units as shown in Figure 2(b). Because the thickness of viscous sublayer is very small, the distribution of oxygen along the thickness direction can be treated to be uniform, the oxygen concentration in each unit is regarded as constant and equal to the oxygen concentration at the unit center. In each unit, the equilibrium potential and exchange current density of cathodic reaction can be calculated according to (3) and (4). If DCC is not considered, the corrosion current (rate) of the wall of the corresponding unit could be got by computing formulas (5) and (6).

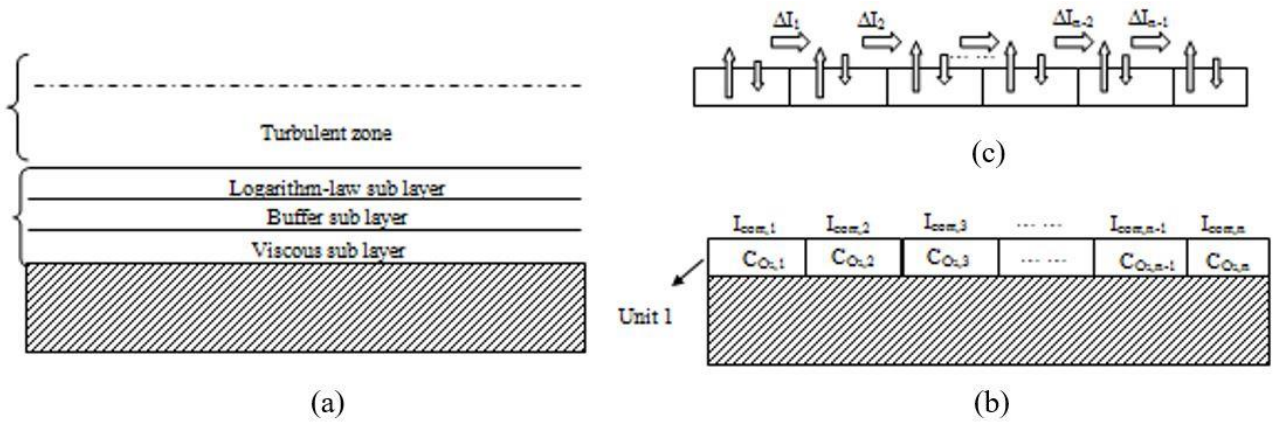

Figure 2. Schematic of the boundary layer and division of viscous sublayer: (a) boundary layers near the wall; (b) units division; and (c) the current flow between units

In fact, the units are not insulated, but connected as a whole. Therefore, the current flow between units is generated under the driving of potential difference, as shown in Figure 3(c). Due to this external current in the cell, the natural corrosion potential is polarized and then the natural corrosion current is changed. If the corrosion potential after polarization can be obtained, DCC mechanism will be identified.

3. CALCULATION OF FLOW FIELD

Before studying the DCC corrosion in Z-shaped pipe, the flow field in the pipe must be solved. The boundary conditions of the flow field are given in Table 3 and Figure 1. The numerical simulation was carried out using FLUENT and calculated results are shown in Figure 3. The pressure distribution shows that the pressure at Zone A is lower than that at zone C and the pressures at Zones B and A are similar. Oxygen does not easily gather in the region with a high pressure, thus the concentration is the highest in Zone A and the lowest in Zone C. The oxygen concentrations in other zones are between them. The difference between the highest and lowest concentrations is nearly twice of the lowest value, forming conditions for differential concentration corrosion.

Table 3. Boundary conditions used in numerical simulation

Inlet velocity, $m.s^{-1}$	Pressure at outlet, Pa	$c_{o_2,0}$, $m^3.m^{-3}$
0.5	1.013×10^5	3.548×10^{-3}

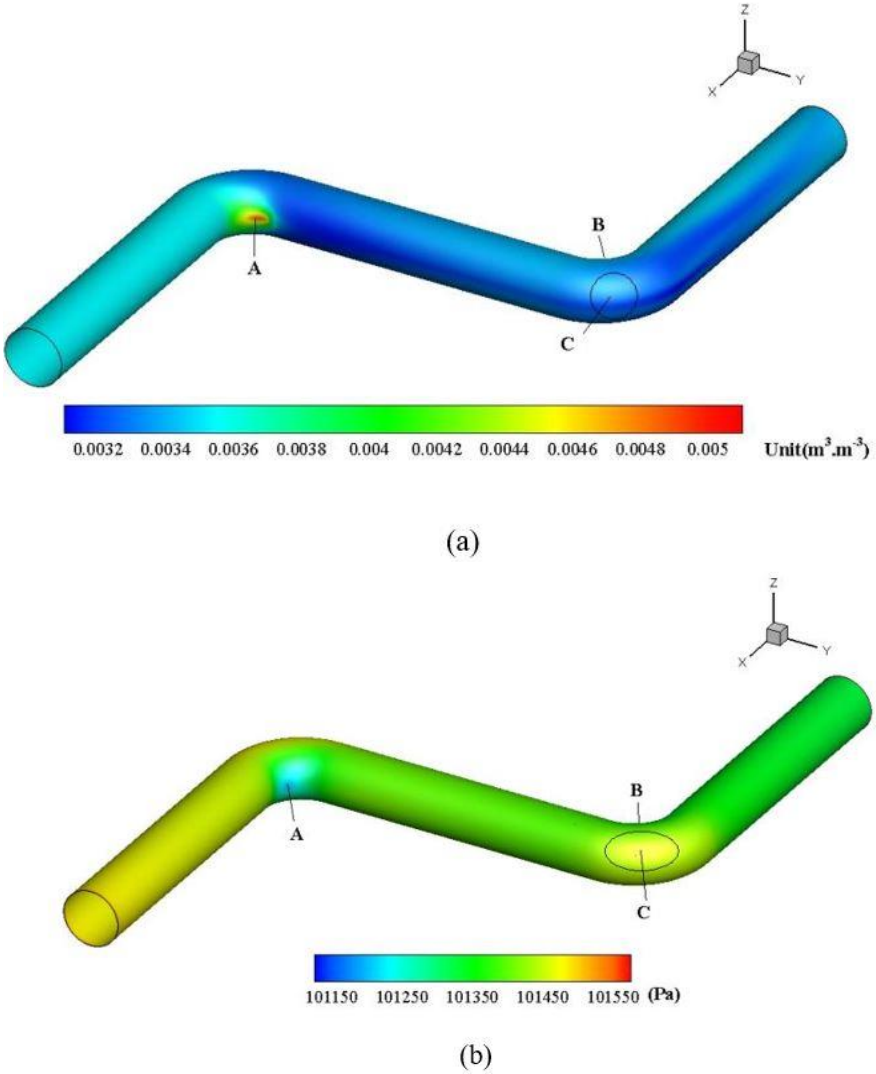

Figure 3. Calculated results on the pipe wall with 0.5 m/s and oxygen concentration 3.548e-3 $m^3.m^{-3}$ at inlet: (a) Distribution of pressure, and (b) distribution of oxygen concentration

4. DIFFERENTIAL CONCENTRATION CORROSION MODEL

4.1. Kirchhoff's Second Law in unit

As described in section 2 ,the viscous sublayer is divided into many units. The oxygen concentration in each unit is constant and equal to that at the unit center, the corresponding natural corrosion potential $E_{corr}^{i,j}$ and current $I_{corr}^{i,j}$ of each unit can be calculated based on Eqs. (3) - (6). Because

of difference of oxygen concentration among units,the $E_{corr}^{i,j}$ is different too. So flowing current among unit will be produced driven by natural corrosion potential difference In this way, polarization occurs in each cell, including polarization of natural corrosion potential $E_{corr}^{i,j}$ and polarization of corrosion current $I_{corr}^{i,j}$, then they all changed. If the corrosion potential and current after polarization can be obtained, the corrosion of DCC would be revealed.

In order to achieve this goal, any representative unit (i, j) is selected in the solution domain as shown in Figure 5. Based on selected representative, the total current flowing into/out of the unit can be expressed as $\sum I_{in}$ and $\sum I_{out}$ .When the corrosion reaches a steady state, According to Kirchhoff's Second Law[16],the unit charge is conserved, i.e. $\sum I_{in} = \sum I_{out}$ .Applying this conservation to all units, a set of discrete equations about the corrosion potential of the unit can be obtained. The corrosion potential in relation to differential concentration corrosion can be firstly calculated by solving these equations, and then the final corrosion current can be obtained. In this regard, the mechanism of concentration corrosion can be clarified.

4.2. Derivation of discrete equations for modeling of DCC

Based on $\sum I_{in} = \sum I_{out}$,the discrete equation of corrosion potential can be derived. Taking unit (i, j) as an example also, in x direction, the current from unit (i, j-1) to unit (i, j) is

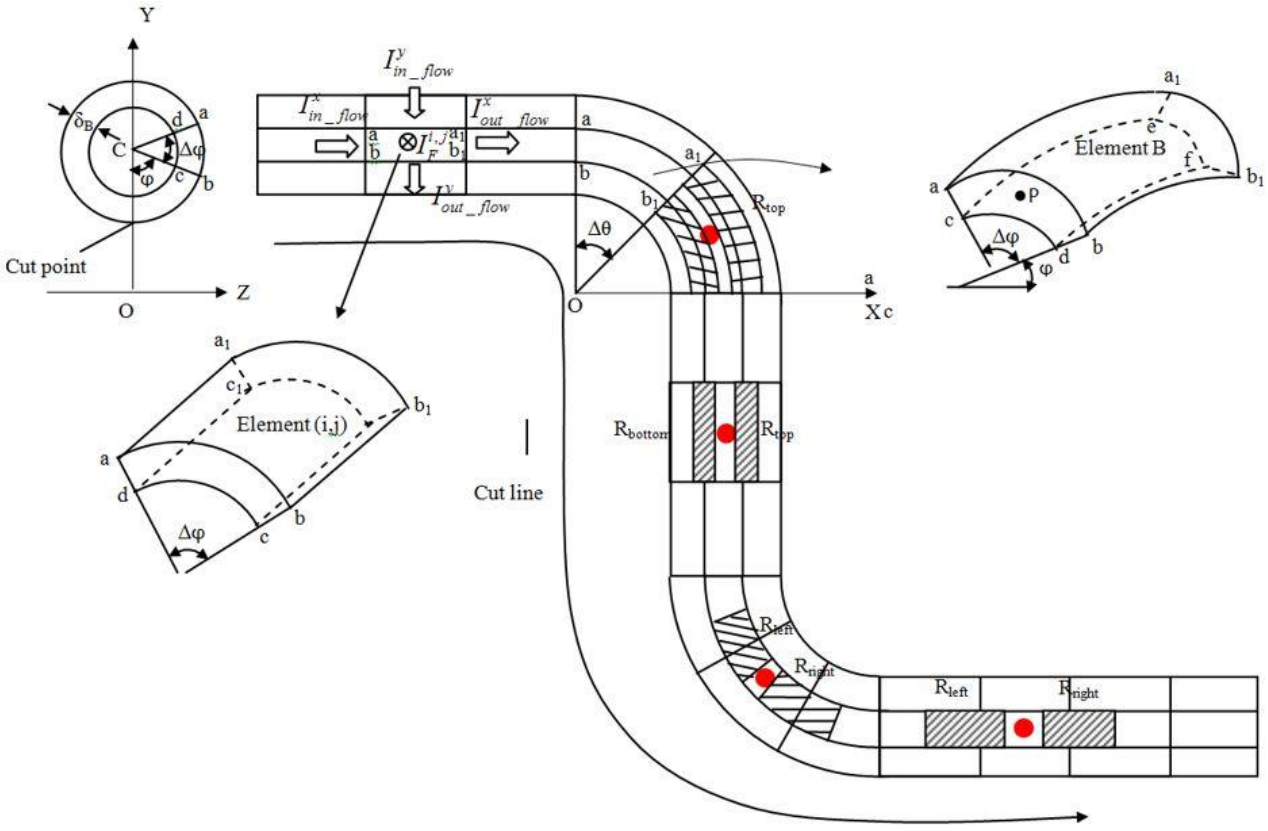

Figure 4. Discretization of computational domain and solution resistance of different parts

$$I^{x}_{in\_flow} = \frac{(-E^{i,j-1}) - (-E^{i,j})}{R_{left}} \tag{7}$$

$E^{i,j}$ is the corrosion potential difference between the wall and the solution after polarization of the natural corrosion potential.

Similarly, the current from unit (i, j) to unit (i, j + 1) is

$$I^{x}_{out\_flow} = \frac{(-E^{i,j}) - (-E^{i,j+1})}{R_{right}} \tag{8}$$

In y direction, the current from the unit (i + 1, j) to the unit (i, j) is

$$I^{y}_{in\_flow} = \frac{(-E^{i+1,j}) - (-E^{i,j})}{R_{top}} \tag{9}$$

Similarly, the current from unit (i, j) to unit (i-1, j) is

$$I^{y}_{out\_flow} = \frac{(-E^{i,j}) - (-E^{i-1,j})}{R_{bottom}} \tag{10}$$

The Farady current due to polarization is

$$I^{i,j}_{F} = \frac{E^{i,j} - E^{i,j}_{corr}}{R^{i,j}_{P}} S \tag{11}$$

where $R_{left}, R_{right}, R_{top}, R_{bottom}$ are the resistances between the unit (i, j) and the neighboring units, which are defined in Figure 4; $R^{i,j}_{P}$ is the polarization resistance of unit (i, j), the corresponding expression is in Section 4.3; S is the contact area between the unit and the wall, for example, aa_1b_1b in Figure 4.

Based on Eqs. (7)-(11), $\sum I_{in} = \sum I_{out}$ for unit (i, j) can be transformed into

$$-\frac{E^{i-1,j}}{R_{bottom}} - \frac{E^{i,j-1}}{R_{left}} + \left(\frac{2}{R_{left}} + \frac{2}{R_{top}} + \frac{2}{R_{right}} + \frac{2}{R_{bottom}} + \frac{S}{R^{i,j}_{P}}\right)E^{i,j} - \frac{E^{i,j+1}}{R_{right}} - \frac{E^{i+1,j}}{R_{top}} = \frac{S}{R^{i,j}_{P}} E^{i,j}_{corr} \tag{12}$$

At the ends of the pipe, Eq. (12) can be simplified because there are insulation conditions, i.e. $I^{x}_{in\_flow} = 0$ and $I^{x}_{out\_flow} = 0$.

A set of discrete equations regarding the corrosion potential are obtained after applying Eq. (12) to each unit in the field. The solution of these equations leads to the final potential distribution in the flow field.

4.3. Calculations of resistance

Each unit, highlighted in red spot, is surrounded by four neighboring units. Resistances between these units exist, defined as R_{left}, R_{right}, R_{bottom}, R_{top} in Figure 4, respectively. In terms of locations and shape characteristics, the units are categorized into two types: (1) units in the straight pipe region, and (2) units in elbow region.

The first type of unit is of regular shape and its resistance can be calculated based on unit (i, j),

$$R_{left} = R_{right} = \rho_s \frac{\Delta x}{S_{abcd}} \tag{13}$$

$$R_{top} = R_{bottom} = \rho_s \frac{R\Delta\varphi}{S_{aa_1cc_1}} \tag{14}$$

Where ΔX is the unit length along the axial direction, ρ_s is the solution resistivity, the reciprocal of a conductivity with value of 4.863S listed in Table 1. Areas can be calculated below,

$$S_{abcd} = \pi[R^2 - (R-\delta)^2]\frac{\Delta\varphi}{2\pi} \approx \delta R\Delta\varphi \tag{15}$$

$$S_{aa_1c_1c} = \delta\Delta x \tag{16}$$

The second type of unit, unit B in Figure 4 as an example, has a complex shape. Therefore, the calculation method is more complicated. The approximate resistances along arc and circumferential directions are given below,

$$R_{left} = R_{right} \approx \rho\,(\overset{\frown}{aa_1} + \overset{\frown}{bb_1})/2S_{abcd} \tag{17}$$

$$R_{top} \approx \rho\frac{R\,\Delta\,\varphi}{S_{aa_1ec}} \tag{18}$$

$$R_{bottom} \approx \rho\frac{R\,\Delta\,\varphi}{S_{bb_1fd}} \tag{19}$$

The polarization resistance between pipe wall and solutions can be calculated by the following formula [14],

$$R_p^{i,j} = \frac{B}{I_{i,j}^{corr}} \tag{20}$$

$$B = \frac{\beta_a\beta_c}{\beta_a + \beta_c} \tag{21}$$

Where β_a, β_c are the Tafel slope of iron and oxygen respectively listed in Table 1.

5. ANALYSIS OF RESULTS

Figure 5(a) shows the distribution of oxygen concentration on the pipe wall. The oxygen concentration is the highest at A (Refer to Figure 4,the same below) and the lowest at C. Figures 5(b), (b_1) and 6(a), (a_1) show that the distribution of natural corrosion potential and current. Corresponding to the oxygen distribution, the natural corrosion potential and current are higher in the region with higher oxygen concentration. However, once DCC is considered, the natural corrosion potential can be polarized. The polarization potential distribution is shown in Figures 5(c) and (c_1). The cathodic polarization occurs at A with higher potential. The potential at A decreases after polarization. Oppositely, the anodic polarization occurs at C with lower potential, which leads to increased potential at C after polarization. Therefore, the overall potential tends to be constant, as shown in Figures 5(d) and (d_1).

The potential polarization leads to the currents in relation to cathode and anode reactions. These currents are not equal, resulting in polarization currents, as shown in Figures 6(b) and (b_1). As a result, the distribution of the final corrosion current changes greatly, and the corrosion current at A decreases while that of C increases.

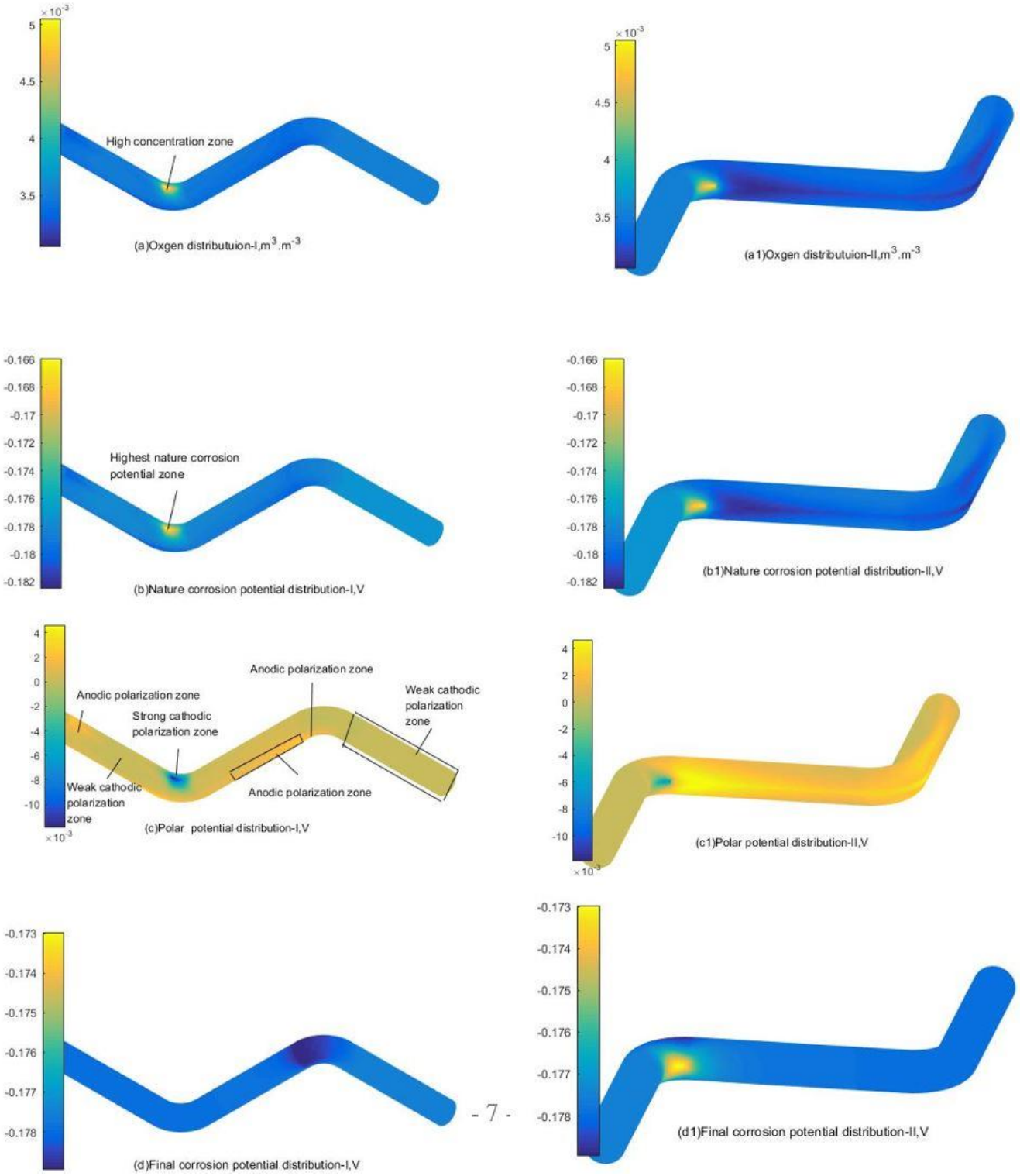

Figure 5. Potential distributions on the pipe wall.

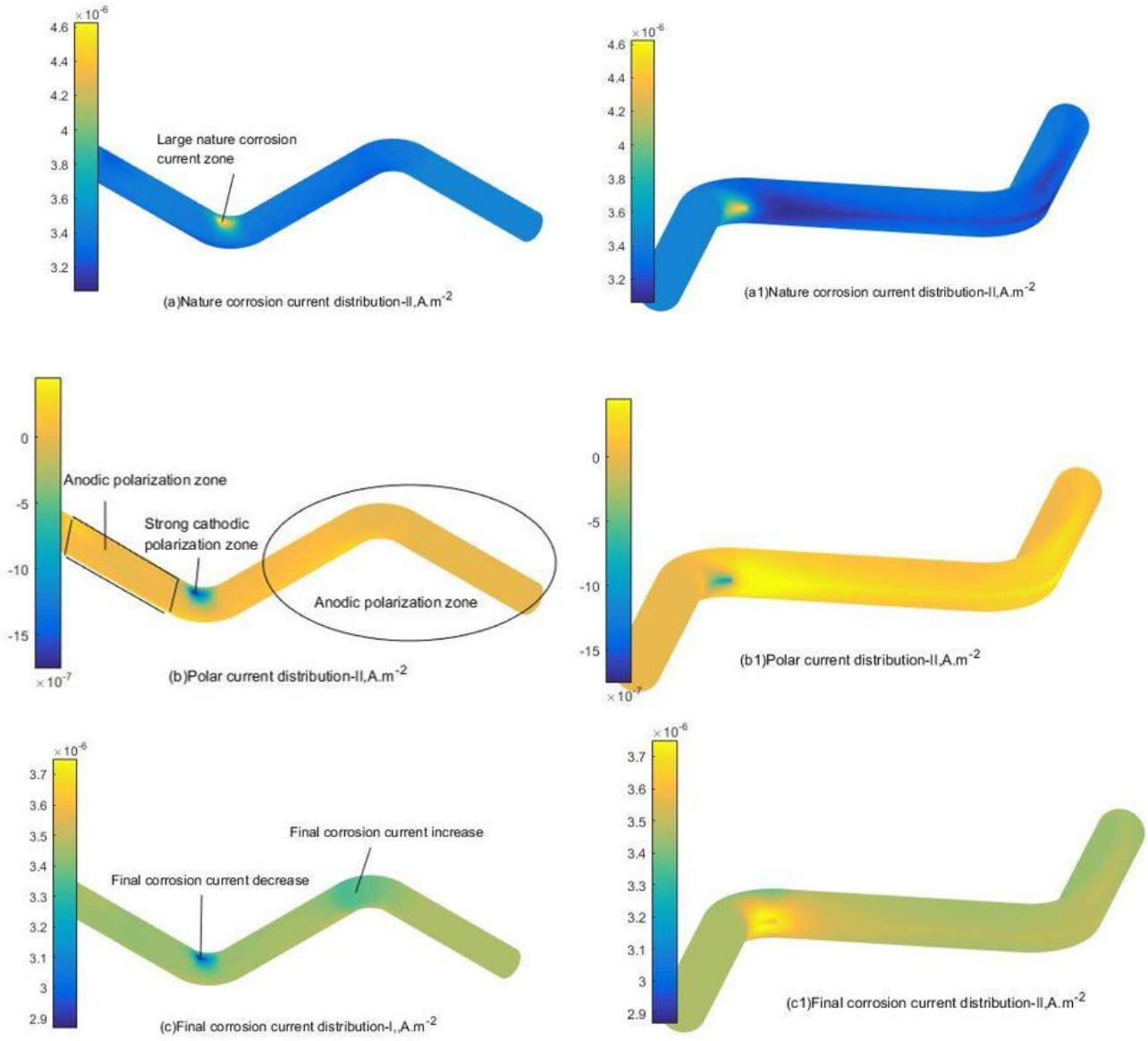

Figure 6. Current distributions on the pipe wall

To further illustrate the corrosion mechanism due to concentration difference, the Z-shaped pipe is cut open at cut point and along cut line (shown in Figure 5), and is then unfolded. Figures 7 and 8 show the current and potential distributions on these unfolded walls, respectively.

Without considering DCC, Figure 8 shows that the corrosion rate at the intrados of pipe elbow is higher than that of the extrados of pipe elbow. This conclusion can be confirmed by the calculation results in reference[17]. In that article,the author calculated the corrosion rate of a series of points on the pipe wall from extrados of pipe elbow to the intrados of pipe elbow on a 45 degree cross section of the bend as shown in Figure 10(a). Because the velocity at the extrados of pipe elbow is lower and that at the intrados of pipe elbow is higher, the different velocities in Figure 9(a) actually represent different points from the extrados of pipe elbow to the intrados of pipe elbow.

From these results, it seems that the intrados of pipe elbow should be destroyed firstly. However,

when DCC is considered, the corrosion rate of the extrados of pipe elbow can be higher than that of intrados of pipe elbow, so that the extrados of pipe elbow should be corroded firstly. Figure 9(b) is cited from reference [17] too, the abscissa has the same meaning with that in Figure 9(a), and the ordinate is the corrosion rate after considering DCC. It can be clearly seen that the smaller the velocity (closer to the extrados of pipe elbow), the higher the corrosion rate. This conclusion is consistent with the conclusion in this paper.

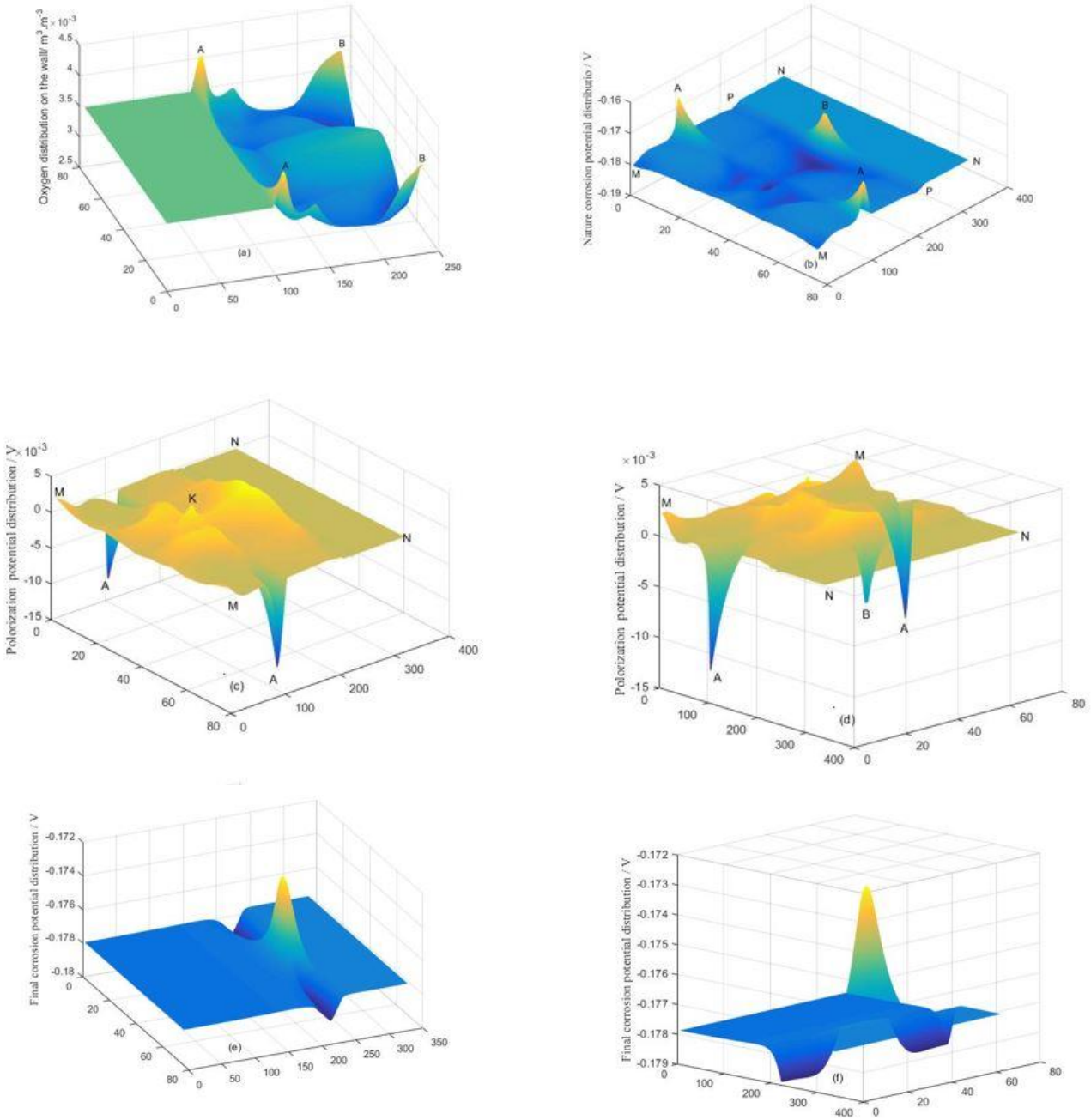

Figure 7. Potential distribution on unfolded wall surface(a) Oxygen distribution (b)Nature corrosion potential distribution (c)Polarization potential distribution from view 1 (d) Polarization potential distribution from view 2(e)Final corrosion potential distribution from view 1 (f) Polarization potential distribution from view 2

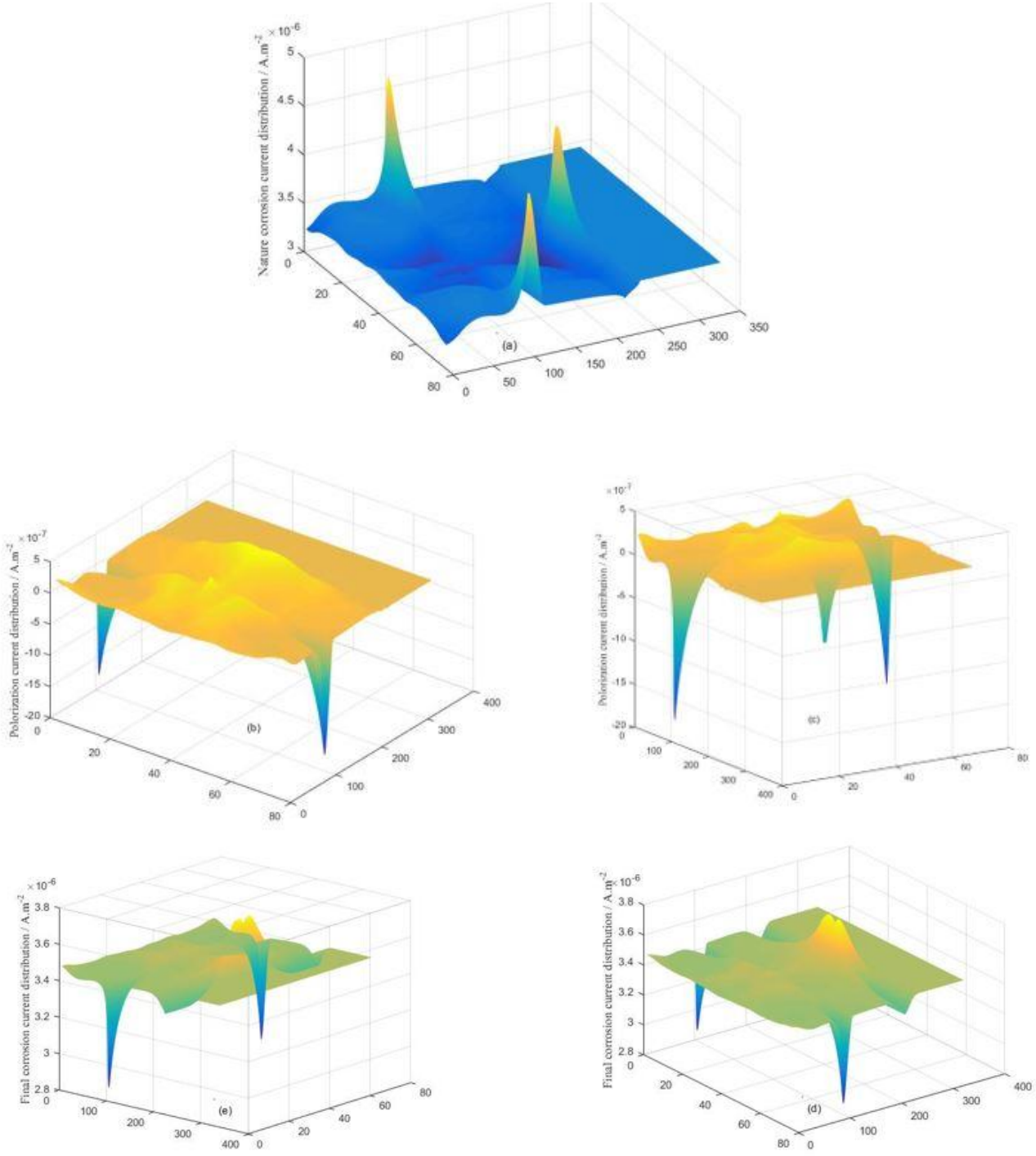

Figure 8. Current distribution on the unfolded wall surface (a)Nature corrosion current distribution (b)Polarization current distribution from view 1 (c) Polarization current distribution from view 2(d)Final corrosion current distribution

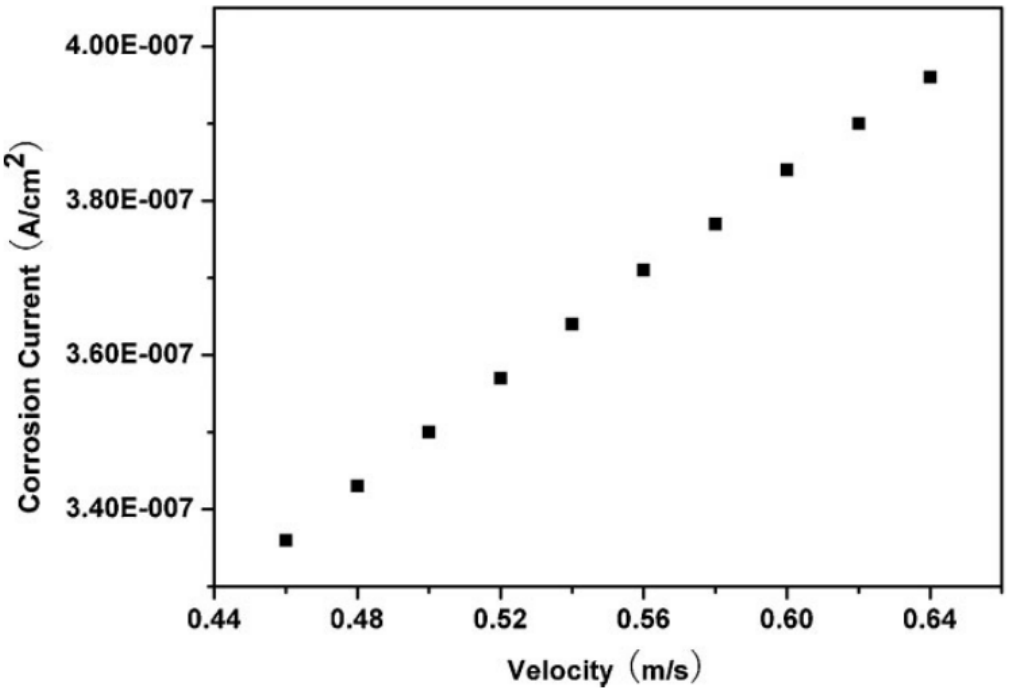

(a)

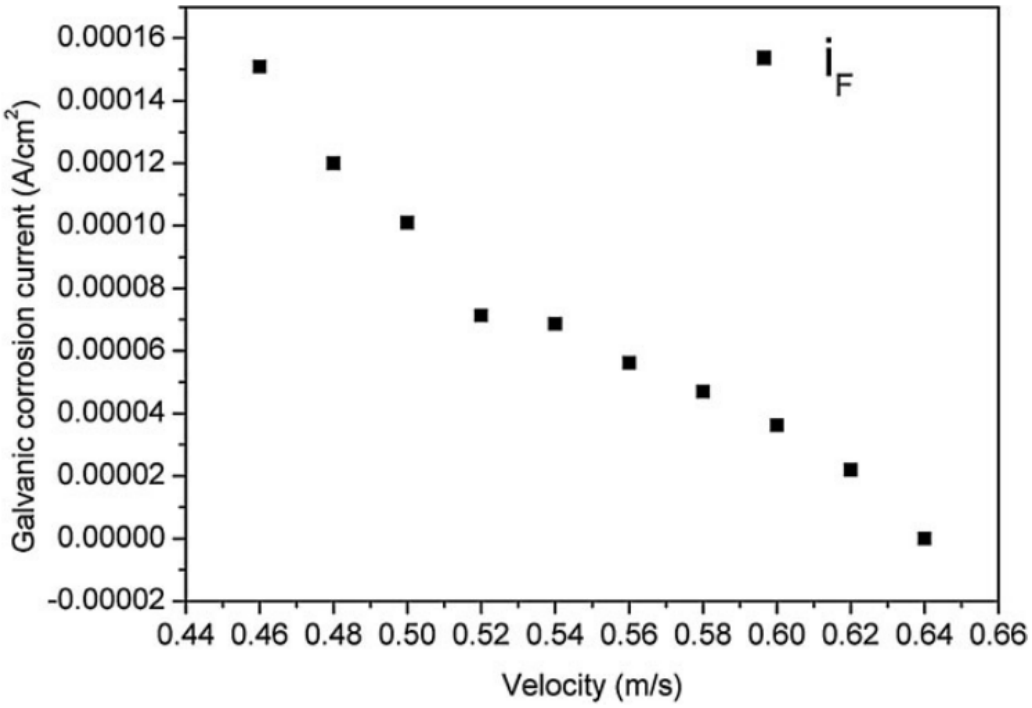

(b)

Figure 9. Calculation results of a one dimensional concentration corrosion model(a) Corrosion rate distribution without considering DCC (b) Corrosion rate distribution considering DCC(Cited from [17])

6. CONCLUSIONS

Differential concentration corrosion can significantly change the distribution of natural corrosion

potential and current at the intrados pipe elbow of a Z-shaped pipe. Based on DCC, the parts with low natural corrosion potential can produce anode polarization, causing the increased potential and accelerated corrosion rate; the parts with high natural corrosion potential can produce cathodic polarization, causing the decreased potential and decelerated corrosion rate. The polarization tends to lead to the homogenization of potential, which is critical for the occurrence of early damage of the extrados of pipe elbow. (need to be specific with one or two sentences to explain why) These findings clarify the corrosion mechanism of elbow in a Z-shaped pipe and can be further applied to other engineering practice with an oxygen concentration distribution.

References

1. F.T. Su,*Journal of Chinese Society Corrosion and Protection*(in chinese), 1(1981)25.
2. Y. Liu, Y.H. Wu and X.L. Song, *Corrosion and Protection,* (in chinese), 29(2008)438.
3. J. De Gruyter, S.F.L. Mertens and E. Temmerman, *J. Electroanal. Chem*, 506(2001)61.
4. Š. Msallamová, P. Novák, M. Kouřil and J. Stoulil, *Mater.Corros.*, 66 (2015)498.
5. J.I. Martins and M.C. Nunes, *Electrochim. Acta* , 52(2006)552.
6. K. Ting and Y.P. Ma, *Nucl.Eng.Des*.,191(1999)231.
7. T.S. Ajmal, Shashi Bhushan Arya and K. Rajendra Udupa, *Int. J. Press. Vessels Pip*. ,174(2019)42.
8. H.P. Rani, T. Divya, R.R. Sahaya,V. Kain and D.K. Baru, *Ann. Nucl. Eng.*,69(2014)351.
9. Korosh Keshtkar,Mohammadreza Nematollahi and Ali Erfaninia, *J. Hydrol. Eng.*, 41(2016)7036.
10. Wael H. Ahmed, *Ann. Nucl. Eng.*,37(2010)598.
11. Y. Utanohara and M. Murase, *Nucl. Eng. Des.*,342(2019)20.
12. X.Y. Yong,Y.Z. Lin,J.J. Liu and Z.P. He, J. Chem. Ind. Eng.(in chinese),2002,53(7) 680.
13. B. Liu and Y.W. Liu ,*Scicntific reports*,10(2020)19236.
14. Thomas L.Floyd and David M. Buchla, Electronics Fundamentals Circuits,Devices,and Applications,Tsinghua University Press,(2014) Beijing,CHINA.
15. C.N. Cao. Principle of corrosion electrochemistry ,Chemical Industry Press,(2004)Beijing,CHINA.
16. Carl H. Hamann, Andrew Hamnett and Wolf Vielstich, Electrochemistry Chemistry Industry Press,(2010)Beijing,CHINA.
17. X.L. Zhu,X.F. Lu and X. Ling, *Mater.Corros.*, 66(2013)498.